applied sciences

MDPI

Article

Magnetically Separable Chiral Periodic Mesoporous Organosilica Nanoparticles

Suheir Omar and Raed Abu-Reziq *

Institute of Chemistry, Casali Center of Applied Chemistry, Center for Nanoscience and Nanotechnology, The Hebrew University of Jerusalem, Jerusalem 9190401, Israel; suheir.omar@mail.huji.ac.il

* Correspondence: Raed.Abu-Reziq@mail.huji.ac.il; Tel.: +97-22-658-6097

Received: 27 July 2020; Accepted: 24 August 2020; Published: 28 August 2020

Abstract: We describe, for the first time, a successful strategy for synthesizing chiral periodic mesoporous organosilica nanoparticles (PMO NPs). The chiral PMO nanoparticles were synthesized in a sol–gel process under mild conditions; their preparation was mediated by hydrolysis and condensation of chiral-bridged organo-alkoxysilane precursor compounds, $(OR')_3Si\text{-}R\text{-}Si(OR')_3$, in the presence of cetyltrimethylammonium bromide (CTAB) surfactant. The resulting nanoparticles were composed merely from a chiral- bridged organo-alkoxysilane monomer. These systems were prepared by applying different surfactants and ligands that finally afforded monodispersed chiral PMO NPs consisting of 100% bridged-organosilane precursor. In addition, the major advancement that was achieved here was, for the first time, success in preparing magnetic chiral PMO NPs. These nanoparticles were synthesized by the co-polymerization of 1,1′-((1*R*,2*R*)-1,2-diphenylethane-1,2-diyl)bis(3-(3-(triethoxysilyl) propyl) urea) chiral monomer by an oil in water (o/w) emulsion process, to afford magnetic chiral PMO NPs with magnetite NPs in their cores. The obtained materials were characterized with high-resolution scanning electron microscopy (HR-SEM), high-resolution transmission electron microscopy (HR-TEM), energy-dispersive X-ray (EDX) spectroscopy, powder X-ray diffraction (XRD), solid-state NMR analysis, circular dichroism (CD) analysis, and nitrogen sorption analysis (N_2-BET).

Keywords: magnetic nanoparticles; chiral materials; periodic mesoporous organosilica; nanoparticles

1. Introduction

Chirality is a fundamental research topic and of vital importance for various fields in natural sciences. Chiral biomolecules have been recognized as the basis of life on earth and many phenomena in nature could be explained through the concepts of stereoisomerism and chirality. In the last decades, the major efforts have been devoted to developing methods for creation and isolation of chiral organic molecules because of their significance in numerous applications [1–3]. Recently, increasing attention has been paid to the construction of chiral solid materials and chiral surfaces due to their potential to be applied in chiral adsorption, enantioseparations and catalysis [4–13]. In particular, several methods have been developed for the fabrication of chiral silica in different morphologies [14–30]. These methods include the utilization of chiral surfactants or polymers as template, the condensation of silane monomers containing chiral organic groups and the grafting of chiral groups on the walls of mesoporous silica materials.

A significant breakthrough in porous materials came in 1999 when three independent research groups discovered periodic mesoporous organosilicas (PMOs) [31–33]. PMO materials soon demonstrated their special position in the field of organic–inorganic hybrid materials [34–39], and were investigated intensively in a wide range of applications such as optical materials, adsorbents, trapping agents, drug delivery agents, and catalyst supports [40–45]. The success of these PMOs is

mainly attributed to their convenient preparation. Within a few years, PMOs with myriad bridging organic groups, narrow distribution pore sizes, and well-defined pore geometries were synthesized and characterized [46–49]. Generally, PMOs are synthesized by a sol–gel process under mild conditions and their preparation is based on the hydrolysis and condensation of bridged organo-alkoxysilane precursor compounds, $(OR)_3Si\text{-}R\text{-}Si(OR)_3$, in the presence of surfactants or block copolymers that assist in creating uniform pores of 2–30 nm size [50–53]. The organic moieties of the PMOs are implemented directly and distributed homogenously within the inorganic walls. This organic hybridization of the silicate network permits precise control over the surface properties, modification of the hydrophilic/hydrophobic character of the surface, alteration of the surface reactivity, protection of the surface from attack, and modification of the bulk properties of these materials [54,55]. The surface area of PMOs can reach up to 1800 m^2/g, which makes these materials particularly attractive for the various applications mentioned above.

The development of chiral PMOs has recently represented a conspicuous success in material sciences [56–61]. Chiral PMOs have also been prepared using chiral organosilane precursors and their potential for different applications was demonstrated in asymmetric catalysis [62–68], chiral chromatography [69,70], and chiral separations [71,72]. Initial attempts to prepare chiral PMOs were based on the co-condensation of chiral bis-alkoxysilane compounds or ligands with tetraalkoxysilane (e.g., tetraethoxysilane) [73–75]. The preparation routes are diverse, including in situ co-polymerization, post-condensation, and immobilization of chiral organic bis-alkoxysilane moieties [76–87]. In addition, novel helical chirally doped PMOs were also reported [15,61]. Usually, the loading of the chiral units into a PMO framework is less than 30% [88–96]. However, the catalytic activity and enantioselectivity of such chiral PMOs in asymmetric transformations is usually less than their homogeneous analogues. For this reason, preparation of chiral PMOs with highly ordered mesostructures, which can exhibit high catalytic activity and chiral induction abilities, is still a challenging research topic. Recently, some reports described the possibility of preparing chiral PMOs constructed only from single enantiopure chiral organosilane precursors. These 100% chiral PMOs represent a unique class of hybrid mesoporous systems, although no catalytic applications have been reported yet [20,22,97–102]. One of the most elegant strategies for preparing chiral catalytic nanosystems is based on supporting metal nanoparticles onto these solid supports.

Magnetic nanoparticles (MNPs) have emerged as a promising class of nanomaterials that have resulted in massive advancements in many biological [103], biomedical [104,105], and catalytic applications [106–111]. Recent studies show that magnetic nanoparticles serve as excellent supports for catalysts [112,113]. The supported catalysts have proved to be effective and easily separated from the reaction media by applying an external magnetic field.

Herein we report a successful method for the preparation of chiral periodic mesoporous organosilica nanoparticles in a sol–gel process under mild conditions. Their preparation was initiated by the synthesis of chiral bis-organosilane precursors that served as chiral building blocks for the formation of chiral PMO NPs. In our project, we succeeded to synthesize and characterize different chiral bridged-silane ligands that were utilized for the preparation of the synthesis attempts were focused on the preparation of pure chiral PMO NPs that were composed merely from a chiral bridged organo-alkoxysilane monomer. The preparation of these systems was accomplished by applying different surfactants and ligands who could finally afford a monodispersed chiral PMO NPs consisted of a 100% bridged-silane precursor. Additionally, for the first time, a successful preparation of magnetic chiral PMO NPs was also accomplished. The PMO nanoparticles were synthesized by a co-polymerization of 1,1′-((1*R*,2*R*)-1,2-diphenylethane-1,2-diyl)bis(3-(3-(triethoxysilyl)propyl)urea) chiral monomer by an o/w emulsion process, to give magnetic chiral PMO NPs with magnetite NPs in their cores.

2. Materials and Methods

2.1. General Information

X-ray powder diffraction (XRD) patterns were obtained using a D8 advanced diffractometer (Bruker AXS, Karlsruhe, Germany) with Cukα radiation. The infrared spectra were recorded using a Perkin Elmer (FTIR 65) spectrometer. Scanning electron microscopy (SEM) was performed using a Sirion SEM microscope (FEI Company), a Schottky-type emission source, and a secondary electron (SE) detector, operated at a voltage of 5 kV. Transmission electron microscopy (TEM), scanning transmission electron microscopy (STEM), and electron diffraction spectroscopy (EDS) were performed with a (S)TEM Tecnai F20 G2 (FEI Company, Fremont, CA, USA) instrument operated at 200 kV. Size distribution and zeta potential determination were performed on a Nano Series instrument, model Nano-Zetasizer ZEN3600 (Malvern Instruments, Malvern, UK). Thermogravimetric analysis (TGA) was performed on a Mettler Toledo TG 50 analyzer. Measurements were carried out at a temperature range that extended from 25 to 900 °C and at a heating rate of 10 °C/min under an inert atmosphere (N_2). The specific surface areas were calculated by means of the Brunauer–Emmett–Teller (BET) equation by utilizing a high-speed gas sorption analyzer, Quantachrome Nova 1200e instrument. Gas chromatography (GC; Agilent Technologies, 7890A) with a universal capillary column (HP-5, 30 m) was used to determine the reactions' conversion and selectivity. Circular dichroism (CD) analyses were recorded with BioLogic instruments using Biokine software under a xenon lamp source on a MOS 500 spectrometer. ^{1}H NMR and ^{13}C NMR spectra were recorded using a Bruker DRX-400 and DRX-500 instrument. Sections 2.2–2.5 are cited from Arakawa et al., 2008 [114].

2.2. Preparation of the Chiral Bridged-Organosilane Ligand (**1**) [Arakawa et al., 2008]

A solution of 4-(2-(trimethoxysilyl)ethyl)benzene-1-sulfonyl chloride (2.5 g, 7.6 mmol) in CH_2Cl_2 (20 mL) was added to a solution of (1*R*,2*R*)-1,2-diphenylethane-1,2-diamine (3.22 g, 15.2 mmol) in CH_2Cl_2 (30 mL) and triethylamine (2.3 mL, 16.8 mmol) at 0 °C. The resulting mixture was stirred for 12 h under nitrogen. After the solvent was evaporated, the crude product was purified by a short column chromatography (ethyl acetate:hexane 1:1) to afford a white solid of R,R-(**1**) (79%). ^{1}H NMR (400 MHz, $CDCl_3$): δ = 0.94 (t, *J* = 5.2 Hz, 4H), 2.69 (t, *J* = 3.2 Hz, 4H), 3.63 (s, 18H), 4.15 (d, *J* = 7.6 Hz, 2H), 4.48 (d, *J* = 5.2 Hz, 2H), 7.29–7.50 (m, 18H); ^{13}C NMR (100 MHz, $CDCl_3$): δ = 18.7, 20.1, 50.4, 56.4, 125.9, 126.3, 127.1, 127.8, 128.2, 141.1, 142.7, 143.5. Elemental analysis: C, 53.2; H, 6.08; N, 3.21; S, 8.72; Si, 6.98.

2.3. Preparation of the Chiral Bridged-Organosilane Ligand (**2**) [Arakawa et al., 2008]

A solution of triethoxy(3-isocyanatopropyl)silane (1.87 g, 7.6 mmol) in CH_2Cl_2 (20 mL) was added to a solution of (1*R*,2*R*)-cyclohexane-1,2-diamine (1.73 g, 15.2 mmol) in CH_2Cl_2 (30 mL) and triethylamine (2.3 mL, 16.8 mmol) at 0 °C. The resulting mixture was stirred for 12 h under nitrogen. After the solvent was evaporated, the crude product was purified by short column chromatography (ethyl acetate:hexane 1:1) to afford a white solid of R,R-(**2**). (67%). ^{1}H NMR (400 MHz, $CDCl_3$): δ = 0.64 (t, *J* = 7.4 Hz, 4H), 1.23 (t, *J* = 5.2 Hz, 20H), 1.54–1.58 (m, 4H), 1.71–1.73 (m, 2H), 2.03–2.06 (m, 2H), 2.18 (s, 2H), 3.02–3.06 (m, 2H), 3.14–3.19 (m, 2H), 3.42–3.52 (m, 2H), 3.65–3.84 (m, 12H), 4.88 (s, 2H), 5.22 (s, 2H); ^{13}C NMR (100 MHz, $CDCl_3$): δ = 7.65, 18.42, 23.58, 24.99, 33.25, 43.01, 54.73, 58.39, 159.03. Elemental analysis: C, 50.79; H, 9.12; N, 9.57; Si, 9.28.

2.4. Preparation of the Chiral Bridged-Organosilane Ligand (**3**) [Arakawa et al., 2008]

A solution of triethoxy(3-isocyanatopropyl)silane (1.87 g, 7.6 mmol) in CH_2Cl_2 (20 mL) was added to a solution of L-Lysine (2.22 g, 15.2 mmol) in CH_2Cl_2 (30 mL) and triethylamine (2.3 mL, 16.8 mmol) at 0 °C. The resulting mixture was stirred for 12 h under nitrogen. After the solvent was evaporated, the crude product was purified by short column chromatography (ethyl acetate:hexane 1:1) to afford a white solid of (**3**) (92%). ^{1}H NMR (400 MHz, $CDCl_3$): δ = 0.63–0.67 (m, 6H), 1.08–1.25 (m, 22H), 1.39–1.67 (m, 6H), 2.56 (s, 2H), 3.16–3.31 (m, 6H), 3.52-3.86 (m, 12H), 4.10 (s, 1H), 4.53 (s, 1H); ^{13}C NMR

(100 MHz, $CDCl_3$): δ = 13.28, 19.07,21.62, 24.83, 28.94, 41.05, 46.28, 58.17, 61.32, 156.82, 160.43, 173.87. Elemental analysis: C, 47.87; H, 8.62; N, 9.08; Si, 8.72.

2.5. Preparation of the Chiral Bridged-Organosilane Ligand (4) [Arakawa et al., 2008]

A solution of triethoxy(3-isocyanatopropyl)silane (1.87 g, 7.6 mmol) in CH_2Cl_2 (20 mL) was added to a solution of (1*R*,2*R*)-1,2-diphenylethane-1,2-diamine (3.22 g, 15.2 mmol) in CH_2Cl_2 (30 mL) and triethylamine (2.3 mL, 16.8 mmol) at 0 °C. The resulting mixture was stirred for 12 h under nitrogen. After the solvent was evaporated, the crude product was purified by short column chromatography (ethyl acetate:hexane 1:1) to afford a white solid of R,R-(**4**). (83%) ^{1}H NMR (400 MHz, $CDCl_3$): δ = 0.609 (t, *J* = 8.4 Hz, 4H), 1.23 (t, *J* = 13.6 Hz, 18H), 1.58 (t, *J* = 7.6 Hz, 4H), 3.07–3.24 (m, 4H), 3.78–3.83 (m, 12H), 5.01 (s, 2H), 5.71 (s, 2H), 7.07–7.17 (m, 10H); ^{13}C NMR (100 MHz, $CDCl_3$): δ = 7.59, 18.28, 23.52, 43.00, 58.40, 60.47, 127.27, 127.41, 128.28, 140.26, 158.73. Elemental analysis: C, 57.64; H, 8.22; N, 7.17; Si, 8.06.

2.6. Preparation of the Chiral PMO Nanoparticles (Chiral PMO NPs)

The chiral PMO nanoparticles were synthesized as follows: CTAB (0.78 g), deionized water (88 mL), and ethanol (33 mL), 25% aqueous ammonia (0.5 mL) were mixed. Then, the chiral organosilane monomer (2.1 mmol), dissolved in 4 mL ethanol, was dropped into the mixture under stirring. The reaction mixture was stirred for 24 h at room temperature. The solid product was then collected by centrifuge and washed in a Soxhlet apparatus using acidic ethanol (1 mL of concentrated HCl in 100 mL of ethanol) for 24 h in order to extract the CTAB surfactant. The obtained chiral PMO NPs were dried at 54 °C for 16 h to afford a fine white-beige powder.

2.7. Preparation of Hydrophobic Magnetite Nanoparticles Coated with Oleic Acid (MNP-OA)

The magnetic nanoparticles were prepared according to the Massart procedure [115]: Briefly, 11.7 g of $FeCl_3{\cdot}6H_2O$ and 4.23 g of $FeCl_2{\cdot}4H_2O$ were dissolved in 400 mL of deionized water under nitrogen gas with vigorous mechanical stirring at 90 °C. At this temperature, 18 mL of concentrated ammonia (25%) were added quickly to the solution, and it was stirred at the same temperature for an extra 20 min. Then, 18 mL of oleic acid was added dropwise to the reaction mixture, and the resulting mixture was stirred at 90 °C for an additional hour. After being cooled to room temperature, a black precipitate was collected by applying an external magnetic field and washing several times with water and acetone. Finally, the hydrophobic magnetite nanoparticles were suspended in 100 mL of chloroform and sonicated for 60 min before further use.

2.8. Preparation of the Magnetic Chiral PMO Nanoparticles (Magnetic Chiral PMO NPs)

Magnetic chiral PMO nanoparticles were synthesized as follows: CTAB (0.78 g), deionized water (88 mL), ethanol (33 mL), and 25% aqueous ammonia (0.5 mL) were mixed. Then, the chiral organosilane monomer (2.1 mmol) dissolved in 4 mL ethanol and 1 mL of hydrophobic magnetite nanoparticles coated with oleic acid (MNP-OA) was dropped into the mixture under stirring. The reaction mixture was mechanically stirred for 24 h at room temperature. The solid product was then collected by a magnet and washed in a Soxhlet apparatus using ethanol for 24 h to extract the CTAB surfactant. The final magnetic chiral PMO NPs were dried at 54 °C for 16 h to afford a fine black-gray powder.

3. Results and Discussion

3.1. Preparation and Characterization of Chiral PMO NPs

The preparation of chiral PMO nanoparticles was initiated by synthesizing a small library of chiral-bridged organosilane monomers that could serve as chiral building blocks of the periodic mesoporous organosilica nanoparticles. These chiral ligands were synthesized by reacting to different chiral amines and amino acids with a silane compound in a molar ratio of 1:2 under an inert atmosphere as illustrated in Scheme 1.

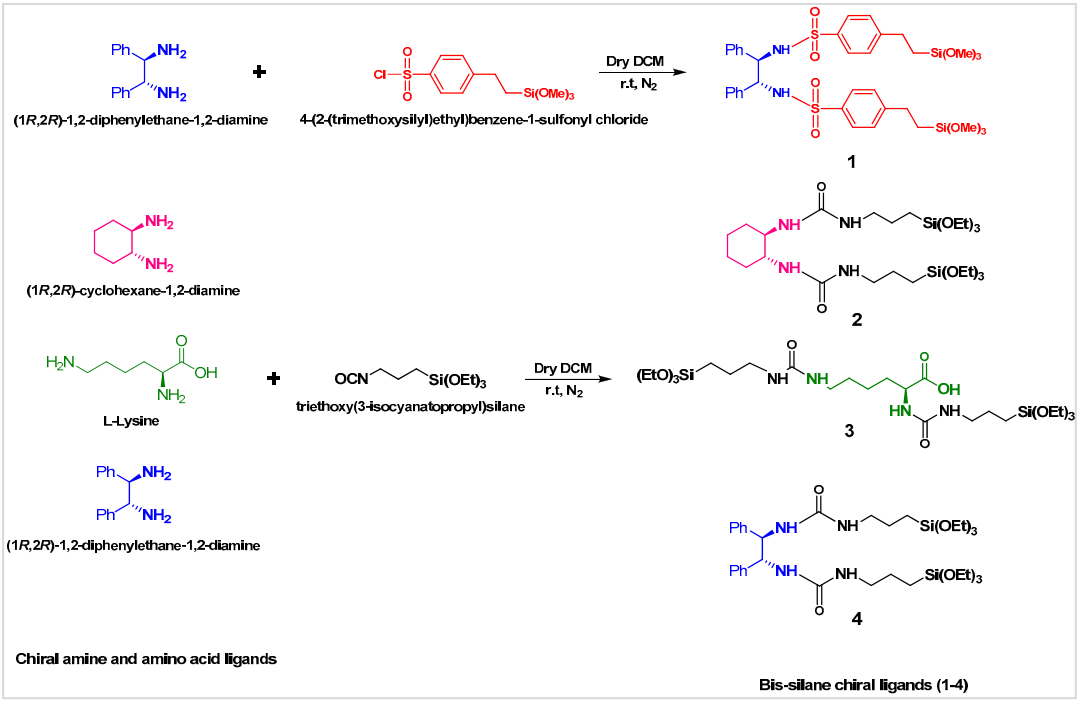

Scheme 1. Synthesis of chiral-bridged organosilane ligands.

After the chiral building blocks were prepared, the chiral PMO NPs were prepared by emulsifying the oil phase containing the chiral-bridged silane precursor in an ethanol/water mixture containing cetyltrimethylammonium bromide (CTAB) or a cetyltrimethylammonium chloride (CTAC) surfactant as a structure-directing agent. Under these conditions, the chiral ligands 1-3 yielded in the presence of CTAB or CTAC either aggregates or fused nanoparticles as was observed by scanning electron microscopy (SEM) analysis (Figures 1–3). On the other hand,1,1′-((*1R,2R*)-1,2-diphenylethane-1,2-diyl)bis(3-(3-(triethoxysilyl)propyl)urea) chiral ligand (**4**) was the best chiral candidate for preparing chiral PMO nanoparticles, which afforded chiral PMO NPs with uniform shape and size as shown in the SEM images (Figure 4). In addition, a representative transmission electron microscopy (TEM) image of this system exhibited very well-ordered spherical nanoparticles with a very low resolution of their mesoporous texture (Figure 4).

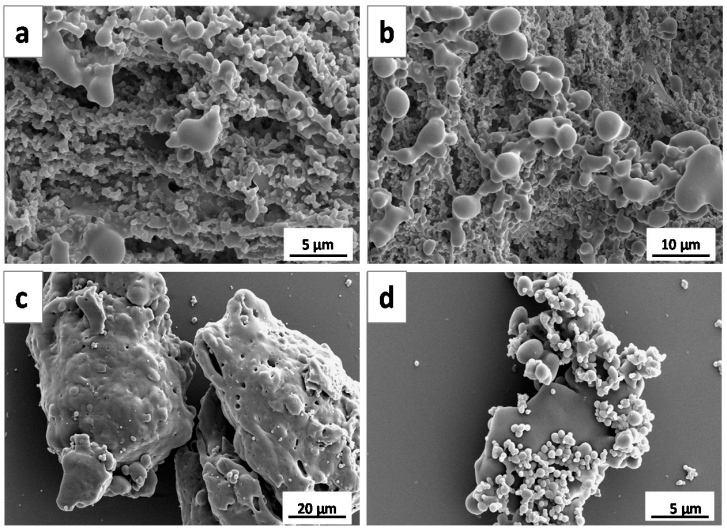

Figure 1. SEM images of a chiral periodic mesoporous organosilica (PMO) system prepared from ligand (**1**) with (**a**,**b**) CTAB and (**c**,**d**) CTAC surfactants.

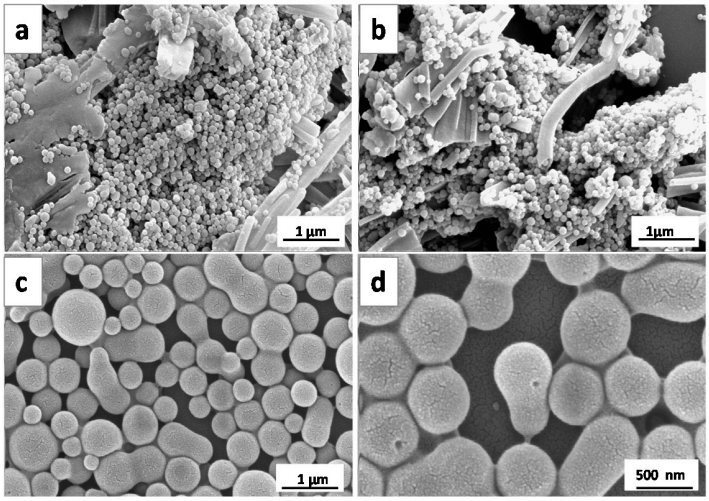

Figure 2. SEM images of a chiral PMO system prepared from ligand (**2**) with (**a**,**b**) CTAB and (**c**,**d**) CTAC surfactants.

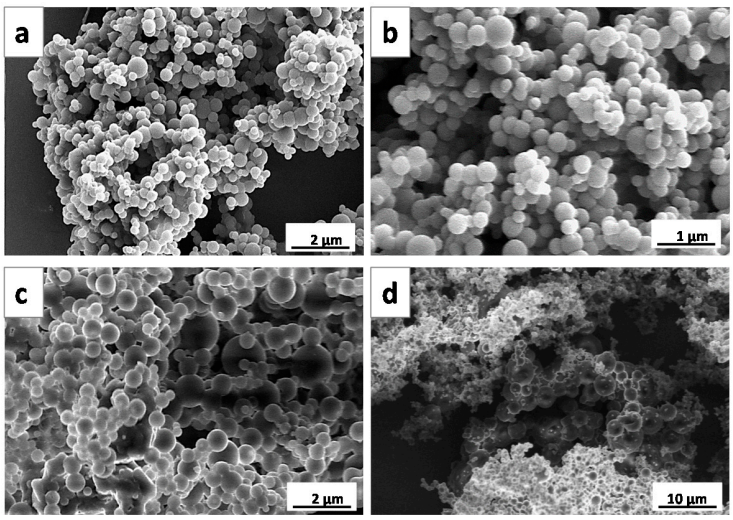

Figure 3. SEM images of a chiral PMO system prepared from ligand (**3**) with (**a**,**b**) CTAB and (**c**,**d**) CTAC surfactants.

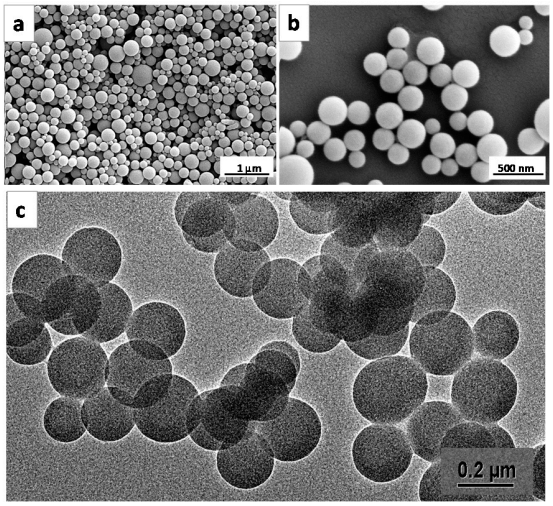

Figure 4. SEM (**a**,**b**) and TEM (**c**) images of a chiral PMO system prepared from ligand (**4**) with CTAB surfactant.

In addition to the cationic surfactants, the contribution of other polymeric surfactants to the system was tested with a ligand (**4**). Apparently, non-ionic and polymeric surfactants were not highly favored in these systems and according to the obtained results, it was concluded that a cationic CTAB surfactant was the best candidate for preparing chiral PMO nanoparticles. The resulting SEM images of different systems that were prepared by utilizing different surfactants are summarized in Table 1. As seen in entries 1-3, when Trition X-100, Igepal CO-520, and Pluronic P123 surfactants were used, nanometric sized PMO NPs were obtained, but they were highly fused and some aggregates were observed. The use of Brij 78 surfactant (Table 1, entry 4) yielded very smooth submicron PMO particles but they were also fused. However, the utilization of a cationic surfactant was much favored because it yields smooth and spherical nanoparticles.

Table 1. Preparation of a chiral PMO system from 1,1′-((*1R,2R*)-1,2-diphenylethane-1,2-diyl)bis(3-(3-(triethoxysilyl)propyl)urea) ligand (**4**) with different surfactants.

Entry	Surfactant	Structure	SEM Images
1.	Triton X-100	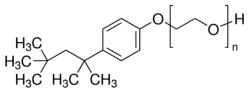	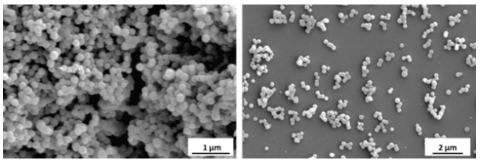
2.	Igepal CO-520	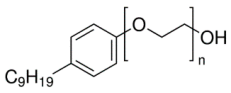	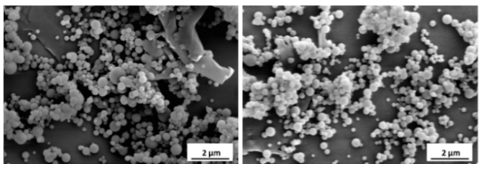
3.	Pluronic P123	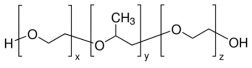	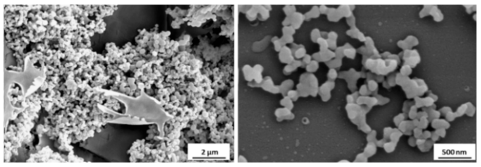
4.	Brij 78	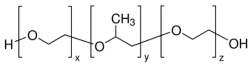	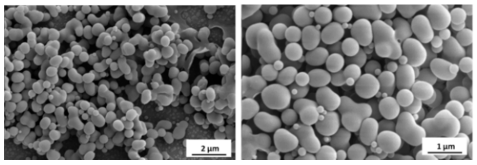
5.	Genamin KDMP	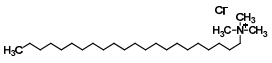	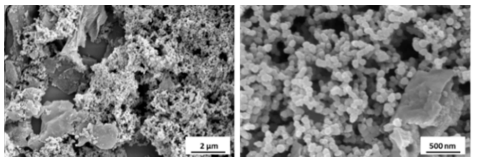
6.	CTAC 25%	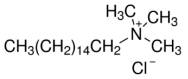	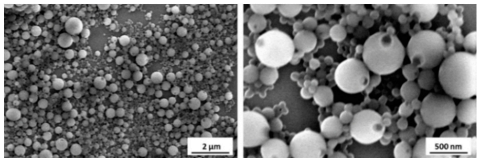
7.	CTAB	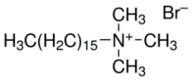	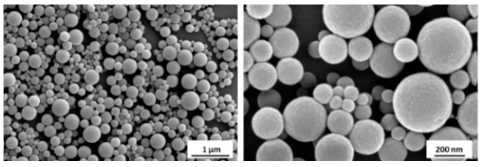

3.2. Preparation and Characterization of Magnetic Chiral PMO NPs

In the same manner, we prepared magnetic chiral PMO NPs based on the same interfacial polycondensation techniques. As illustrated in Scheme 2, the hydrophobic magnetic nanoparticles, together with the chiral-bridged organosilane ligand (**4**), were added to the aqueous phase, which includes water, ethanol, and ammonium hydroxide (25%). By the end of this sol–gel process, spherical nanoparticles composed of 100% bridging chiral organosilane monomers filled with magnetite (Fe_3O_4) in their cores were formed.

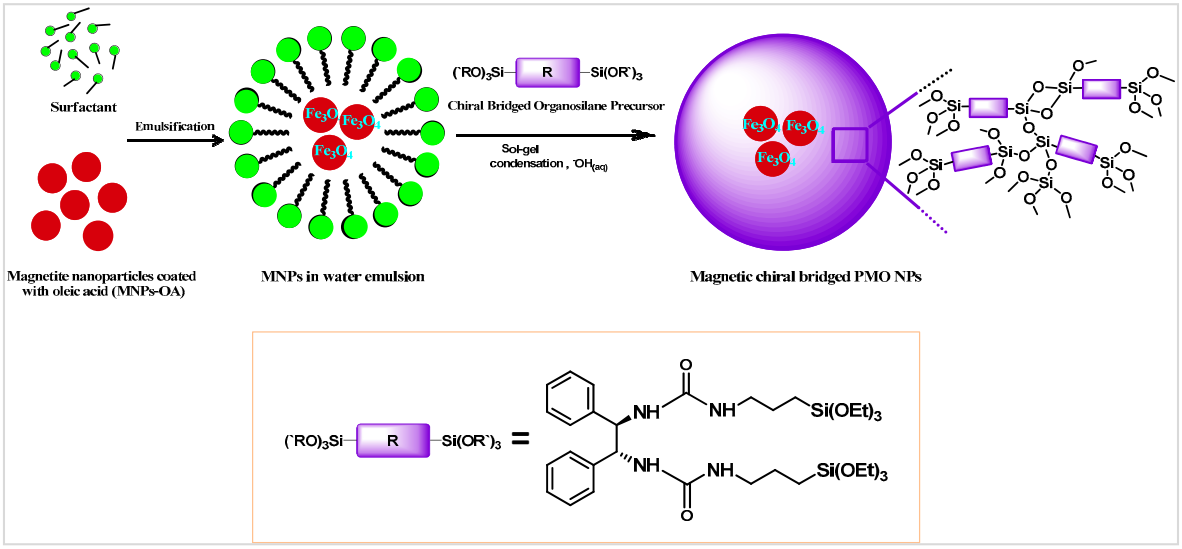

Scheme 2. Preparation of magnetic chiral PMO nanoparticles.

The resulting nanoparticles were analyzed by TEM and STEM spectroscopy, accompanied by energy-dispersive X-ray analysis (EDX). The representative TEM and STEM images in Figure 5 provided clear evidence of the special composition and ordering of the magnetite nanoparticles inside the core of the spherical nanoparticles. Moreover, the EDX spectrum confirms the elemental composition of the obtained chiral magnetic nanoparticles because it exhibits all the relevant peaks of carbon, nitrogen, oxygen, silicon, and iron in the detected organosilica network.

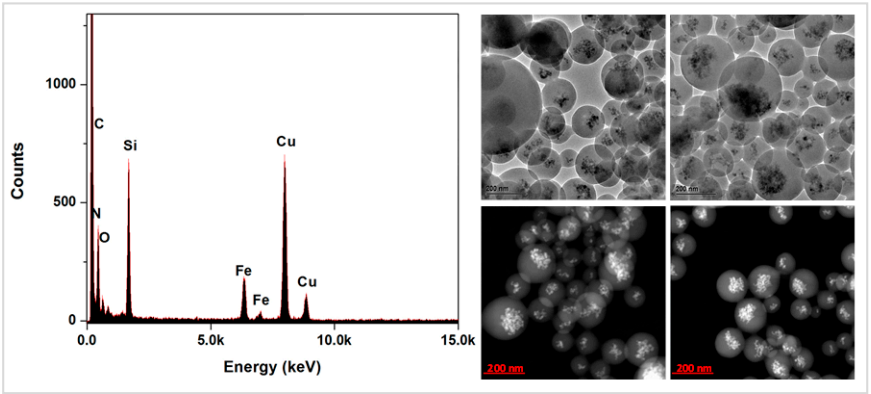

Figure 5. Energy-dispersive X-ray analysis (EDX) (**left**) and TEM-STEM (**right**) analysis of magnetic chiral PMO nanoparticles.

Further elemental determination was conducted by X-ray powder diffraction (XRD) analysis utilized for identifying the structure of this system. The XRD pattern of the magnetic PMO nanoparticles (Figure 6) showed characteristic peaks of magnetite nanoparticles at 2θ = 30.3, 35.7, 43, 53.8, 57.6,

and 63.4, in addition to a sharp peak at 2θ = 1.8–2.7, which is attributed to the mesoscopic structure of the PMO nanoparticles.

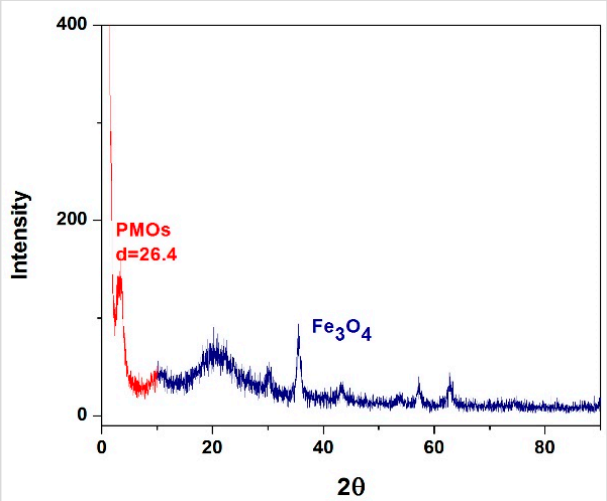

Figure 6. XRD analysis of magnetic chiral PMO nanoparticles.

In addition, EDX-mapping analysis was also utilized to confirm the chemical composition and elemental distribution in our system. Figure 7 presents a homogeneous distribution of oxygen, carbon, and silicon throughout the organosilica network. With nitrogen, a similar distribution was also observed in a lower density. The magnetic naoparticles were concentrated in the core, which it was clearly confirmed by their narrow and specific distribution in the center of the resulting chiral PMO NPs.

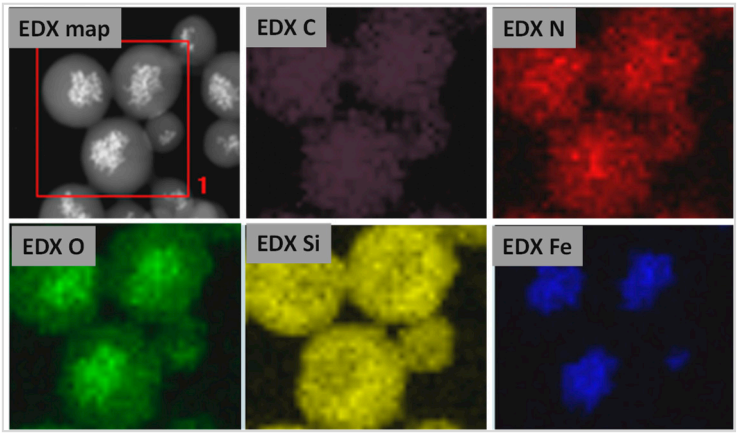

Figure 7. EDX-mapping analysis of magnetic chiral PMO nanoparticles.

The average size of both systems was determined by dynamic light scattering (DLS) analysis, which revealed an average size of 173 nm of the chiral PMO NPs and an average size distribution of 190 nm for the magnetic chiral PMO NPs (Figure 8).

The N_2 adsorption–desorption isotherms of the chiral PMO NPs and the magnetic chiral PMO NPs (Figure 9) exhibit typical IV-type curves that indicate narrow pore sizes with uniform mesopores. The Brunauer–Emmett–Teller (BET) surface area of chiral PMO NPs was estimated to be 497 m^2/g, and the calculated total pore volume was 0.39 $cm^3\ g^{-1}$, whereas the BET surface area of magnetic chiral PMO NPs was estimated to be 371 m^2/g, and the calculated total pore volume was 0.23 $cm^3\ g^{-1}$. These values are indeed quite large considering the low porosity of the resulting nanoparticles and the existence of Fe_3O_4 cores.

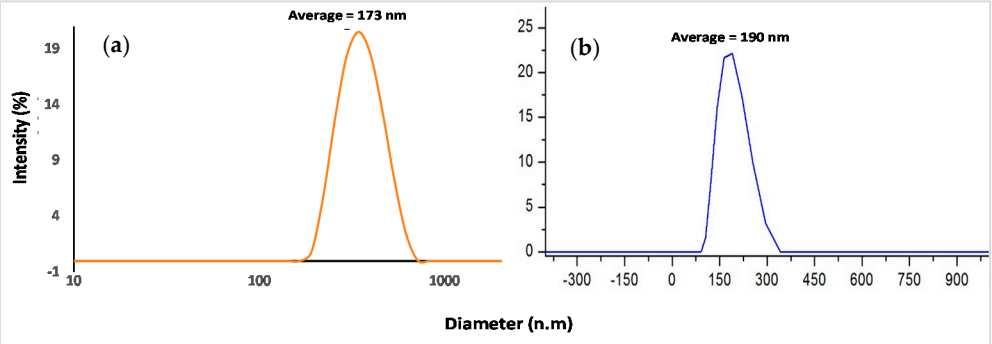

Figure 8. (**a**) Size distribution of chiral PMO nanoparticles (NPs) and (**b**) Size distribution of magnetic chiral PMO NPs.

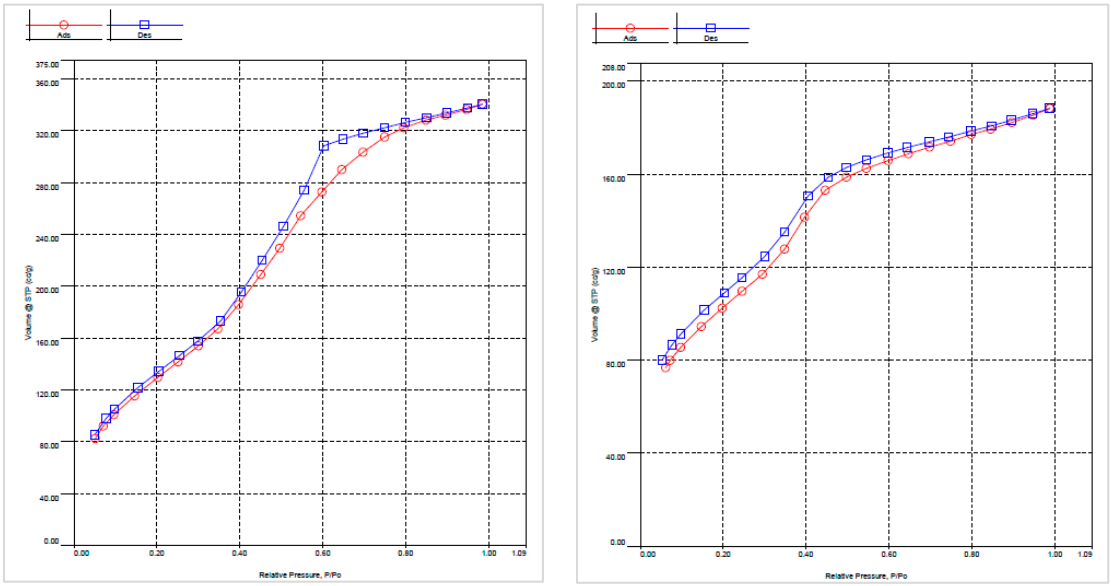

(**a**) (**b**)

Figure 9. N_2 adsorption–desorption isotherms of (**a**) chiral PMO NPs and (**b**) magnetic chiral PMO NPs.

The chemical composition of the magnetic chiral PMO NPs was further characterized by solid-state ^{29}Si and ^{13}C cross-polarization/magic angle spinning(CP-MAS) NMR spectroscopy. This analysis was conducted after treatment with concentrated HCl, which was used for dissolving all the magnetite nanoparticles in the detected system. The ^{29}Si NMR spectrum in Figure 10 exhibited a T^3 value of −67.11 ppm, which confirms the formation of the Si-C covalent bonds in the organosilica framework. In addition, the ^{13}C NMR spectrum of the chiral PMO NPs in Figure 10b gives clear evidence of the successful synthesis of these nanoparticles from ligand (**4**) because it shows all the characteristic peaks of the incorporated ligands between 10 and 66 ppm, in addition to the aromatic species, ranging from 122 to 147 ppm, and a characteristic carbonyl peak of the urea group at 167 ppm. These results clearly indicate the formation of silsesquioxane frameworks and further demonstrate the incorporation of organic units into the silica networks.

FT-IR spectroscopy was employed for determining the chemical composition of chiral PMO NPs and magnetic chiral PMO NPs. Figure 11 compares the FTIR spectra of both systems to the ligand (**4**). Both systems were similar, displaying equivalent peaks that determine the organic content of the chiral-bridged organosilane ligand (**4**) in addition to the distinct absorbance peaks at 1023, 1100, and 1283 cm^{-1}, which can be assigned to Si-C vibrations. Moreover, the absorption bands at intervals of 3120–3700 cm^{-1} in both curves b and c are assigned to the Si-OH stretching vibrations in the resulting silica network. The absorbance peaks at 2790–3100 cm^{-1} are assigned to C-H stretching from both

chiral systems. The presence of the oleate group coating on the magnetite nanoparticles can be barely observed, since its C-H and C=C stretching bands overlap with the distinct IR bands of the original chiral ligand.

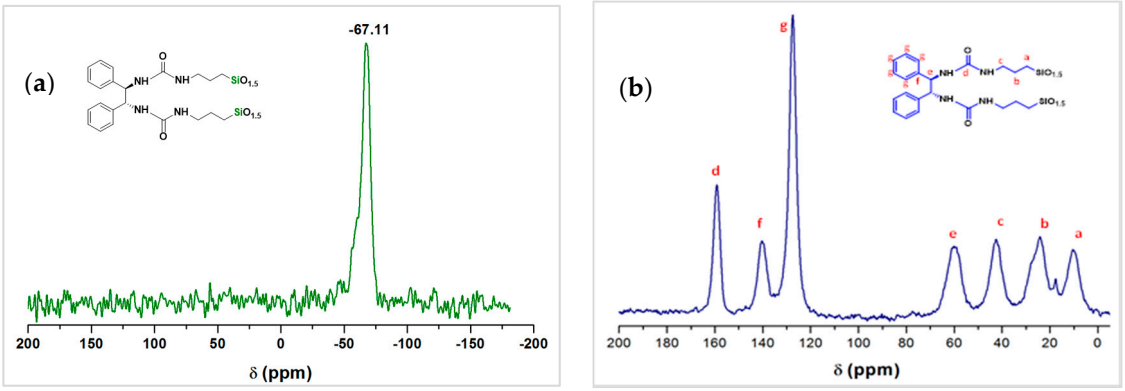

Figure 10. (**a**) Solid-state ^{29}Si CP-MAS NMR spectroscopy of chiral PMO NPs and (**b**) solid state ^{13}C CP-MAS NMR spectroscopy of chiral PMO NPs.

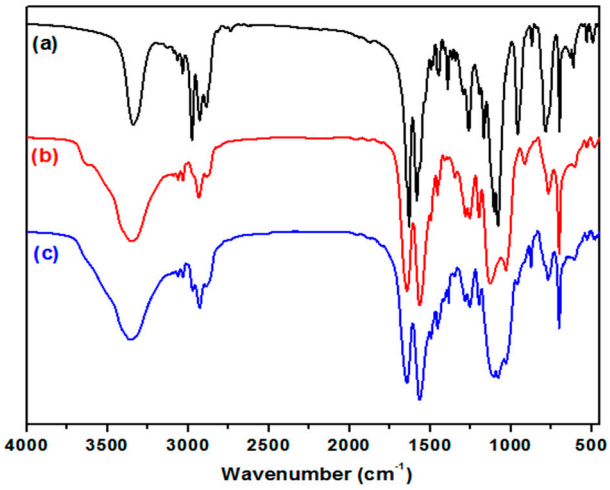

Figure 11. FTIR analysis of (**a**) chiral ligand (**4**), (**b**) chiral PMO NPs, and (**c**) chiral magnetic PMO NPs.

The synthesis of chiral PMO NPs and magnetic chiral NPs was also evident by following the organic contents in the resulting system in comparison to the as-synthesized MNP-OA nanoparticles by thermogravimetric analysis (TGA). In both systems, a slight decomposition occurred in the temperature range of 50–100 °C that could have resulted from ethanol and water residues in the detected system, and the major decomposition process that occurred between 150 and 600 °C. In Figure 12 curve a, a total weight loss of 19.2% was detected with MNP-OA, whereas chiral PMO NPs afforded a total organic loss of 68.2% (Figure 12, curve b), compared with 75.1% with magnetic chiral PMO NPs (Figure 12, curve c). These findings confirm the successful incorporation of the chiral ligand and the magnetic cores besides the good thermal stability of the synthesized chiral systems.

Circular dichroism (CD) spectra of chiral compounds are quite sensitive to their chemical and physical changes. From this spectroscopic method, we would be able to study and prove the chiral character of the as-synthesized chiral PMO NPs compared to a bare chiral bridged-silane ligand (**4**). As seen in Figure 13, the CD spectra of the free ligand (curve a) and the condensed ligand (curve b) are quite similar, with a slight absorbance shift that resulted from its entrapment within the silicate framework.

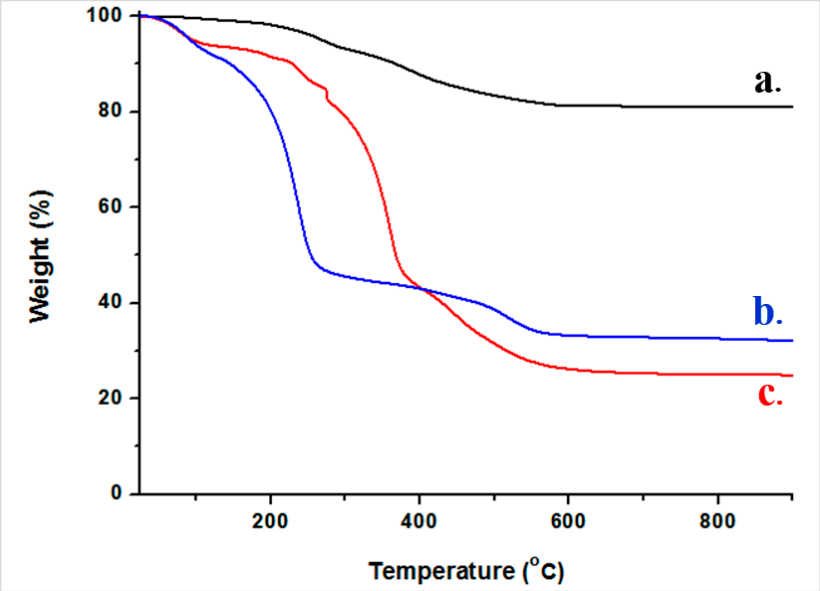

Figure 12. TGA analysis of (**a**) hydrophobic magnetite nanoparticles coated with oleic acid (MNP-OA), (**b**) chiral PMO NPs, and (**c**) chiral magnetic PMO NPs.

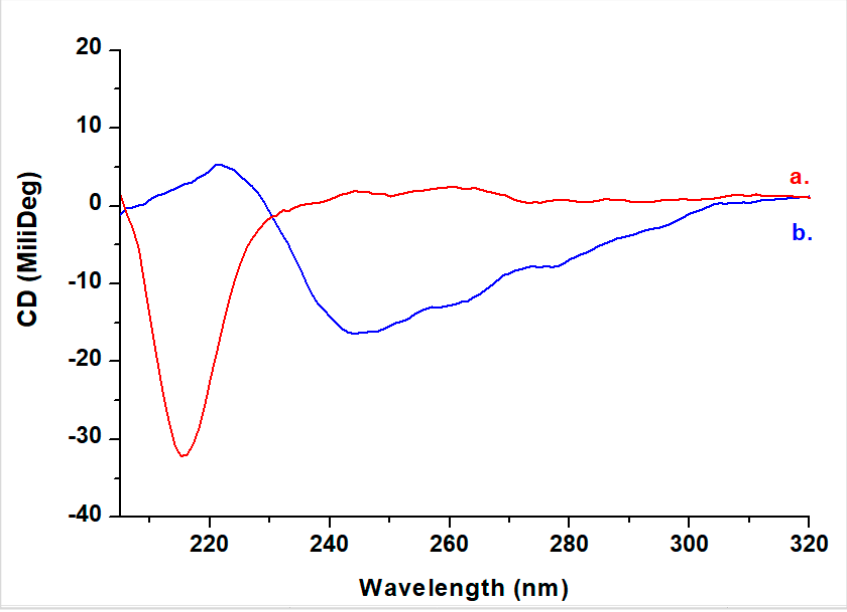

Figure 13. Circular dichroism spectra of (**a**) chiral ligand (**4**) and (**b**) chiral PMO NPs.

4. Conclusions

In this work pure chiral PMO nanoparticles were successfully synthesized using 1,1′-((1R,2R)-1,2-diphenylethane-1,2-diyl)bis(3-(3-(triethoxysilyl) propyl) urea) chiral monomer by co-polymerization and sol–gel condensations. Additionally, magnetic chiral PMO NPs with magnetite nanoparticles in their cores were synthesized for the first time using similar synthetic conditions. We believe that this facile way for preparing chiral catalysts can open new doors for preparing diverse chiral PMO nanocatalysts loaded with different metal nanoparticles that can be highly welcomed in many enantioselective reactions.

Author Contributions: Conceptualization, R.A.-R.; methodology, R.A.-R. and S.O.; formal analysis, R.A.-R. and S.O.; investigation, S.O.; resources, R.A.-R.; data curation, S.O.; writing—original draft preparation, S.O.;

writing—review and editing, R.A.-R. and S.O.; visualization, S.O.; supervision R.A.-R.; project administration, R.A.-R.; funding acquisition, R.A.-R. All authors have read and agreed to the published version of the manuscript.

Funding: This research was funded by Casali Foundation.

Acknowledgments: S. Omar is grateful to the Ministry of Science and Technology of Israel for her fellowship.

Conflicts of Interest: The authors declare no conflict of interest. The funders had no role in the design of the study; in the collection, analyses, or interpretation of data; in the writing of the manuscript, or in the decision to publish the results.

References

1. Gruttadauria, M.; Giacalone, F. (Eds.) *Catalytic Methods in Asymmetric Synthesis*; John Wiley and Sons: Hoboken, NJ, USA, 2011.
2. Subramanian, G. (Ed.) *Chiral Separation Techniques: A Practical Approach*; Wiley-VCH: Weinheim, Germany, 2001.
3. Sheldon, R.A. Chirotechnology: Designing economic chiral syntheses. *J. Chem. Technol. Biotechnol.* **1996**, *67*, 1–14. [CrossRef]
4. Wang, Y.; Xu, J.; Wang, Y.; Chen, H. Emerging chirality in nanoscience. *Chem. Soc. Rev.* **2013**, *42*, 2930–2962. [CrossRef] [PubMed]
5. Song, C.; Liu, X.; Liu, D.; Ren, C.; Yang, W.; Deng, J. Optically Active Particles of Chiral Polymers. *Macromol. Rapid Commun.* **2013**, *34*, 1426–1445. [CrossRef] [PubMed]
6. Yoon, M.; Srirambalaji, R.; Kim, K. Homochiral Metal-Organic Frameworks for Asymmetric Heterogeneous Catalysis. *Chem. Rev.* **2012**, *112*, 1196–1231. [CrossRef]
7. Paik, P.; Mastai, Y.; Kityk, I.; Rakus, P.; Gedanken, A. Synthesis of amino acid block-copolymer imprinted chiral mesoporous silica and its acoustically-induced optical Kerr effects. *J. Solid State Chem.* **2012**, *192*, 127–131. [CrossRef]
8. Paik, P.; Gedanken, A.; Mastai, Y. Chiral-mesoporous-polypyrrole nanoparticles: Its chiral recognition abilities and use in enantioselective separation. *J. Mater. Chem.* **2010**, *20*, 4085–4093. [CrossRef]
9. Morris, R.E.; Bu, X. Induction of chiral porous solids containing only achiral building blocks. *Nat. Chem.* **2010**, *2*, 353–361. [CrossRef]
10. Raval, R. Chiral expression from molecular assemblies at metal surfaces: Insights from surface science techniques. *Chem. Soc. Rev.* **2009**, *38*, 707–721. [CrossRef]
11. Mastai, Y. Enantioselective crystallization on nanochiral surfaces. *Chem. Soc. Rev.* **2009**, *38*, 772–780. [CrossRef]
12. Harris, K.D.M.; Thomas, S.J.M. Selected Thoughts on Chiral Crystals, Chiral Surfaces, and Asymmetric Heterogeneous Catalysis. *ChemCatChem* **2009**, *1*, 223–231. [CrossRef]
13. Marx, S.; Avnir, D. The Induction of Chirality in Sol-Gel Materials. *Acc. Chem. Res.* **2007**, *40*, 768–776. [CrossRef] [PubMed]
14. Jin, R.-H.; Yao, D.-D.; Levi, R. Biomimetic Synthesis of Shaped and Chiral Silica Entities Templated by Organic Objective Materials. *Chem. Eur. J.* **2014**, *20*, 7196–7214. [CrossRef] [PubMed]
15. Garcia-Munoz, R.A.; Morales, V.; Linares, M.; Rico-Oller, B. Synthesis of Helical and Supplementary Chirally Doped PMO Materials. Suitable Catalysts for Asymmetric Synthesis. *Langmuir* **2014**, *30*, 881–890. [CrossRef] [PubMed]
16. Matsukizono, H.; Jin, R.-H. High-Temperature-Resistant Chiral Silica Generated on Chiral Crystalline Templates at Neutral pH and Ambient Conditions. *Angew. Chem. Int. Ed.* **2012**, *51*, 5862–5865. [CrossRef]
17. Qiu, H.; Che, S. Chiral mesoporous silica: Chiral construction and imprinting via cooperative self-assembly of amphiphiles and silica precursors. *Chem. Soc. Rev.* **2011**, *40*, 1259–1268. [CrossRef]
18. Liu, X.; Zhuang, W.; Li, B.; Wu, L.; Wang, S.; Li, Y.; Yang, Y. Helical periodic mesoporous 1,4-phenylene-silica nanorods with chiral crystalline walls. *Chem. Commun.* **2011**, *47*, 7215–7217. [CrossRef]
19. Han, L.; Chen, Q.; Wang, Y.; Gao, C.; Che, S. Synthesis of amino group functionalized monodispersed mesoporous silica nanospheres using anionic surfactant. *Microporous Mesoporous Mater.* **2011**, *139*, 94–103. [CrossRef]
20. Kuschel, A.; Polarz, S. Effects of Primary and Secondary Surface Groups in Enantioselective Catalysis Using Nanoporous Materials with Chiral Walls. *J. Am. Chem. Soc.* **2010**, *132*, 6558–6565. [CrossRef]

21. Wu, X.; Ji, S.; Li, Y.; Li, B.; Zhu, X.; Hanabusa, K.; Yang, Y. Helical Transfer through Nonlocal Interactions. *J. Am. Chem. Soc.* **2009**, *131*, 5986–5993. [CrossRef]
22. Kuschel, A.; Sievers, H.; Polarz, S. Amino acid silica hybrid materials with mesoporous structure and enantiopure surfaces. *Angew. Chem. Int. Ed.* **2008**, *47*, 9513–9517. [CrossRef]
23. Jin, H.; Qiu, H.; Sakamoto, Y.; Shu, P.; Terasaki, O.; Che, S. Mesoporous silicas by self-assembly of lipid molecules: Ribbon, hollow sphere, and chiral materials. *Chem. Eur. J.* **2008**, *14*, 6413–6420. [CrossRef] [PubMed]
24. Chen, H.; He, J. Fine control over the morphology and structure of mesoporous silica nanomaterials by a dual-templating approach. *Chem. Commun.* **2008**, 4422–4424. [CrossRef] [PubMed]
25. Lin, G.-L.; Tsai, Y.-H.; Lin, H.-P.; Tang, C.-Y.; Lin, C.-Y. Synthesis of Mesoporous Silica Helical Fibers Using a Catanionic-Neutral Ternary Surfactant in a Highly Dilute Silica Solution: Biomimetic Silicification. *Langmuir* **2007**, *23*, 4115–4119. [CrossRef]
26. Gabashvili, A.; Medina, D.D.; Gedanken, A.; Mastai, Y. Templating Mesoporous Silica with Chiral Block Copolymers and Its Application for Enantioselective Separation. *J. Phys. Chem. B* **2007**, *111*, 11105–11110. [CrossRef]
27. Yang, Y.; Suzuki, M.; Owa, S.; Shirai, H.; Hanabusa, K. Preparation of helical nanostructures using chiral cationic surfactants. *Chem. Commun.* **2005**, 4462–4464. [CrossRef] [PubMed]
28. Ohsuna, T.; Liu, Z.; Che, S.; Terasaki, O. Characterization of chiral mesoporous materials by transmission electron microscopy. *Small* **2005**, *1*, 233–237. [CrossRef] [PubMed]
29. Che, S.; Liu, Z.; Ohsuna, T.; Sakamoto, K.; Terasaki, O.; Tatsumi, T. Synthesis and characterization of chiral mesoporous silica. *Nature* **2004**, *429*, 281–284. [CrossRef]
30. Kresge, C.T.; Leonowicz, M.E.; Roth, W.J.; Vartuli, J.C.; Beck, J.S. Ordered mesoporous molecular sieves synthesized by a liquid-crystal template mechanism. *Nature* **1992**, *359*, 710–712. [CrossRef]
31. Asefa, T.; MacLachlan, M.J.; Coombs, N.; Ozin, G.A. Periodic mesoporous organosilicas with organic groups inside the channel walls. *Nature* **1999**, *402*, 867–871. [CrossRef]
32. Inagaki, S.; Guan, S.; Fukushima, Y.; Ohsuna, T.; Terasaki, O. Novel Mesoporous Materials with a Uniform Distribution of Organic Groups and Inorganic Oxide in Their Frameworks. *J. Am. Chem. Soc.* **1999**, *121*, 9611–9614. [CrossRef]
33. Melde, B.J.; Holland, B.T.; Blanford, C.F.; Stein, A. Mesoporous Sieves with Unified Hybrid Inorganic/Organic Frameworks. *Chem. Mater.* **1999**, *11*, 3302–3308. [CrossRef]
34. Sayari, A.; Hamoudi, S.; Yang, Y.; Moudrakovski, I.L.; Ripmeester, J.R. New Insights into the Synthesis, Morphology, and Growth of Periodic Mesoporous Organosilicas. *Chem. Mater.* **2000**, *12*, 3857–3863. [CrossRef]
35. Sharma, R.K.; Das, S.; Maitra, A. Surface modified ormosil nanoparticles. *J. Colloid Interface Sci.* **2004**, *277*, 342–346. [CrossRef] [PubMed]
36. Hatton, B.; Landskron, K.; Whitnall, W.; Perovic, D.; Ozin, G.A. Past, Present, and Future of Periodic Mesoporous OrganosilicasThe PMOs. *Acc. Chem. Res.* **2005**, *38*, 305–312. [CrossRef] [PubMed]
37. Qiao, S.Z.; Lin, C.X.; Jin, Y.; Li, Z.; Yan, Z.; Hao, Z.; Huang, Y.; Lu, G.Q. Surface-Functionalized Periodic Mesoporous Organosilica Hollow Spheres. *J. Phys. Chem. C* **2009**, *113*, 8673–8682. [CrossRef]
38. Wang, W.; Lofgreen, J.E.; Ozin, G.A. Mesoporous materials: Why PMO? Towards Functionality and Utility of Periodic Mesoporous Organosilicas (Small 23/2010). *Small* **2010**, *6*, 2621. [CrossRef]
39. Asefa, T.; Coombs, N.; Grondey, H.; Jaroniec, M.; Kruk, M.; MacLachlan, M.J.; Ozin, G.A. Bio-inspired nanocomposites: From synthesis toward potential applications. *Mater. Res. Soc. Symp. Proc.* **2002**, *707*, 93–104.
40. Shea, K.J.; Loy, D.A. Bridged Polysilsesquioxanes. Molecular-Engineered Hybrid Organic–Inorganic Materials. *Chem. Mater.* **2001**, *13*, 3306–3319. [CrossRef]
41. Descalzo, A.B.; Martínez-Máñez, R.; Sancenón, F.; Hoffmann, K.; Rurack, K. The Supramolecular Chemistry of Organic–Inorganic Hybrid Materials. *Angew. Chem. Int. Ed.* **2006**, *45*, 5924–5948. [CrossRef]
42. Shylesh, S.; Samuel, P.; Sisodiya, S.; Singh, A.P. Periodic Mesoporous Silicas and Organosilicas: An Overview Towards Catalysis. *Catal. Surv. Asia* **2008**, *12*, 266–282. [CrossRef]
43. Park, S.; Moorthy, M.; Ha, C.-S. Periodic mesoporous organosilica (PMO) for catalytic applications. *Korean J. Chem. Eng.* **2014**, *31*, 1707–1719. [CrossRef]
44. Gao, J.; Zhang, X.; Xu, S.; Tan, F.; Li, X.; Zhang, Y.; Qu, Z.; Quan, X.; Liu, J. Clickable Periodic Mesoporous Organosilicas: Synthesis, Click Reactions, and Adsorption of Antibiotics. *Chem. Eur. J.* **2014**, *20*, 1957–1963. [CrossRef] [PubMed]

45. Park, S.S.; Santha Moorthy, M.; Ha, C.-S. Periodic mesoporous organosilicas for advanced applications. *NPG Asia Mater.* **2014**, *6*, e96. [CrossRef]
46. Hunks, W.J.; Ozin, G.A. Challenges and advances in the chemistry of periodic mesoporous organosilicas (PMOs). *J. Mater. Chem.* **2005**, *15*, 3716–3724. [CrossRef]
47. Thomas, A. Functional Materials: From Hard to Soft Porous Frameworks. *Angew. Chem. Int. Ed.* **2010**, *49*, 8328–8344. [CrossRef]
48. Waki, M.; Mizoshita, N.; Tani, T.; Inagaki, S. Periodic Mesoporous Organosilica Derivatives Bearing a High Density of Metal Complexes on Pore Surfaces. *Angew. Chem.* **2011**, *123*, 11871–11875. [CrossRef]
49. Hoffmann, F.; Froba, M. Vitalising porous inorganic silica networks with organic functions-PMOs and related hybrid materials. *Chem. Soc. Rev.* **2011**, *40*, 608–620. [CrossRef]
50. Kruk, M. Access to Ultralarge-Pore Ordered Mesoporous Materials through Selection of Surfactant/Swelling-Agent Micellar Templates. *Acc. Chem. Res.* **2012**, *45*, 1678–1687. [CrossRef]
51. Guo, W.; Zhao, X.S. Room-temperature synthesis of hydrothermally stable aluminum-rich periodic mesoporous organosilicas with wormlike pore channels. *Microporous Mesoporous Mater.* **2005**, *85*, 32–38. [CrossRef]
52. Fujita, S.; Inagaki, S. Self-Organization of Organosilica Solids with Molecular-Scale and Mesoscale Periodicities†. *Chem. Mater.* **2008**, *20*, 891–908. [CrossRef]
53. Hoffmann, F.; Cornelius, M.; Morell, J.; Fröba, M. Silica-Based Mesoporous Organic–Inorganic Hybrid Materials. *Angew. Chem. Int. Ed.* **2006**, *45*, 3216–3251. [CrossRef] [PubMed]
54. Melero, J.A.; van Grieken, R.; Morales, G. Advances in the Synthesis and Catalytic Applications of Organosulfonic-Functionalized Mesostructured Materials. *Chem. Rev.* **2006**, *106*, 3790–3812. [CrossRef] [PubMed]
55. Van Der Voort, P.; Esquivel, D.; De Canck, E.; Goethals, F.; Van Driessche, I.; Romero-Salguero, F.J. Periodic Mesoporous Organosilicas: From simple to complex bridges; a comprehensive overview of functions, morphologies and applications. *Chem. Soc. Rev.* **2013**, *42*, 3913–3955. [CrossRef]
56. Yang, Q.; Liu, J.; Zhang, L. Functionalized periodic mesoporous organosilicas: Hierarchical and chiral materials. *Sci. China Chem.* **2010**, *53*, 351–356. [CrossRef]
57. Garcia, R.A.; Morales, V.; Garces, T. One-step synthesis of a thioester chiral PMO and its use as a catalyst in asymmetric oxidation reactions. *J. Mater. Chem.* **2012**, *22*, 2607–2615. [CrossRef]
58. Hoffmann, F.; Cornelius, M.; Morell, J.; Fröba, M. Periodic Mesoporous Organosilicas (PMOs): Past, Present, and Future. *J. Nanosci. Nanotechnol.* **2006**, *6*, 265–288. [CrossRef]
59. Jayalakshmi, V.; Wood, T.; Basu, R.; Du, J.; Blackburn, T.; Rosenblatt, C.; Crudden, C.M.; Lemieux, R.P. Probing the pore structure of a chiral periodic mesoporous organosilica using liquid crystals. *J. Mater. Chem.* **2012**, *22*, 15255–15261. [CrossRef]
60. Meng, X.; Yokoi, T.; Lu, D.; Tatsumi, T. Synthesis and characterization of chiral periodic mesoporous organosilicas. *Angew. Chem. Int. Ed.* **2007**, *46*, 7796–7798. [CrossRef]
61. Wu, X.; Blackburn, T.; Webb, J.D.; Garcia-Bennett, A.E.; Crudden, C.M. The Synthesis of Chiral Periodic Organosilica Materials with Ultrasmall Mesopores. *Angew. Chem. Int. Ed.* **2011**, *50*, 8095–8099. [CrossRef]
62. Yang, Q.; Han, D.; Yang, H.; Li, C. Asymmetric Catalysis with Metal Complexes in Nanoreactors. *Chem. Asian J.* **2008**, *3*, 1214–1229. [CrossRef]
63. Seki, T.; McEleney, K.; Crudden, C.M. Enantioselective catalysis with a chiral, phosphane-containing PMO material. *Chem. Commun.* **2012**, *48*, 6369–6371. [CrossRef] [PubMed]
64. Chen, C.; Kong, L.; Cheng, T.; Jin, R.; Liu, G. Facile construction of functionalized periodic mesoporous organosilica for Ir-catalyzed enantioselective reduction of α-cyanoacetophenones and α-nitroacetophenones. *Chem. Commun.* **2014**, *50*, 10891–10893. [CrossRef]
65. Yang, Q.; Liu, J.; Zhang, L.; Li, C. Functionalized periodic mesoporous organosilicas for catalysis. *J. Mater. Chem.* **2009**, *19*, 1945–1955. [CrossRef]
66. Liu, R.; Jin, R.; An, J.; Zhao, Q.; Cheng, T.; Liu, G. Hollow-Shell-Structured Nanospheres: A Recoverable Heterogeneous Catalyst for Rhodium-Catalyzed Tandem Reduction/Lactonization of Ethyl 2-Acylarylcarboxylates to Chiral Phthalides. *Chem. Asian J.* **2014**, *9*, 1388–1394. [CrossRef] [PubMed]
67. Jiang, D.; Gao, J.; Yang, Q.; Yang, J.; Li, C. Large-Pore Mesoporous Organosilicas Functionalized with trans-(1R,2R)-Diaminocyclohexane: Synthesis, Postmodification, and Catalysis. *Chem. Mater.* **2006**, *18*, 6012–6018. [CrossRef]

68. Liu, K.; Jin, R.; Cheng, T.; Xu, X.; Gao, F.; Liu, G.; Li, H. Functionalized periodic mesoporous organosilica: A highly enantioselective catalyst for the Michael addition of 1,3-dicarbonyl compounds to nitroalkenes. *Chem. Eur. J.* **2012**, *18*, 15546–15553. [CrossRef]
69. Zhou, J.; Du, Q.; Sun, F.; Zheng, X.; Chen, S.; Luo, P. Quinine derivative bonded the hybrid mesoporous silicas chiral stationary phase: Preparation and application in liquid chromatography. *J. Chin. Chem. Soc.* **2015**, *62*, 647–651. [CrossRef]
70. Zhu, G.; Jiang, D.; Yang, Q.; Yang, J.; Li, C. Trans-(1R,2R)-Diaminocyclohexane-functionalized mesoporous organosilica spheres as chiral stationary phase. *J. Chromatogr. A* **2007**, *1149*, 219–227. [CrossRef]
71. Zhu, G.; Zhong, H.; Yang, Q.; Li, C. Chiral mesoporous organosilica spheres: Synthesis and chiral separation capacity. *Microporous Mesoporous Mater.* **2008**, *116*, 36–43. [CrossRef]
72. Ran, R.; You, L.; Di, B.; Hao, W.; Su, M.; Yan, F.; Huang, L. A novel chiral mesoporous binaphthyl-silicas: Preparation, characterization, and application in HPLC. *J. Sep. Sci.* **2012**, *35*, 1854–1862. [CrossRef]
73. Wang, P.; Yang, J.; Liu, J.; Zhang, L.; Yang, Q. Chiral mesoporous organosilicas with R-(+)-Binol integrated in the framework. *Microporous Mesoporous Mater.* **2009**, *117*, 91–97. [CrossRef]
74. MacQuarrie, S.; Thompson, M.P.; Blanc, A.; Mosey, N.J.; Lemieux, R.P.; Crudden, C.M. Chiral Periodic Mesoporous Organosilicates Based on Axially Chiral Monomers: Transmission of Chirality in the Solid State. *J. Am. Chem. Soc.* **2008**, *130*, 14099–14101. [CrossRef] [PubMed]
75. Huang, J.; Zhu, F.; He, W.; Zhang, F.; Wang, W.; Li, H. Periodic Mesoporous Organometallic Silicas with Unary or Binary Organometals inside the Channel Walls as Active and Reusable Catalysts in Aqueous Organic Reactions. *J. Am. Chem. Soc.* **2010**, *132*, 1492–1493. [CrossRef] [PubMed]
76. MacLean, M.W.A.; Wood, T.K.; Wu, G.; Lemieux, R.P.; Crudden, C.M. Chiral Periodic Mesoporous Organosilicas: Probing Chiral Induction in the Solid State. *Chem. Mater.* **2014**, *26*, 5852–5859. [CrossRef]
77. Garcia, R.A.; van Grieken, R.; Iglesias, J.; Morales, V.; Villajos, N. Facile one-pot approach to the synthesis of chiral periodic mesoporous organosilicas SBA-15-type materials. *J. Catal.* **2010**, *274*, 221–227. [CrossRef]
78. Morales, V.; Villajos, J.A.; Garcia, R.A. Simultaneous synthesis of modified Binol-periodic mesoporous organosilica SBA-15 type material. Application as catalysts in asymmetric sulfoxidation reactions. *J. Mater. Sci.* **2013**, *48*, 5990–6000. [CrossRef]
79. Álvaro, M.; Benitez, M.; Das, D.; Ferrer, B.; García, H. Synthesis of Chiral Periodic Mesoporous Silicas (ChiMO) of MCM-41 Type with Binaphthyl and Cyclohexadiyl Groups Incorporated in the Framework and Direct Measurement of Their Optical Activity. *Chem. Mater.* **2004**, *16*, 2222–2228. [CrossRef]
80. Jin, R.; Liu, K.; Xia, D.; Qian, Q.; Liu, G.; Li, H. Enantioselective Addition of Malonates and β-Keto Esters to Nitroalkenes over an Organonickel-Functionalized Periodic Mesoporous Organosilica. *Adv. Synth. Catal.* **2012**, *354*, 3265–3274. [CrossRef]
81. Xia, X.; Wu, M.; Jin, R.; Cheng, T.; Liu, G. One-pot relay reduction-isomerization of β-trifluoromethylated-α,β-unsaturated ketones to chiral β-trifluoromethylated saturated ketones over combined catalysts in aqueous medium. *Green Chem.* **2015**, *17*, 3916–3922. [CrossRef]
82. Liu, R.; Jin, R.; Kong, L.; Wang, J.; Chen, C.; Cheng, T.; Liu, G. Organorhodium-Functionalized Periodic Mesoporous Organosilica: High Hydrophobicity Promotes Asymmetric Transfer Hydrogenation in Aqueous Medium. *Chem. Asian J.* **2013**, *8*, 3108–3115. [CrossRef]
83. Gao, X.; Liu, R.; Zhang, D.; Wu, M.; Cheng, T.; Liu, G. Phenylene-Coated Magnetic Nanoparticles that Boost Aqueous Asymmetric Transfer Hydrogenation Reactions. *Chem. Eur. J.* **2014**, *20*, 1515–1519. [CrossRef] [PubMed]
84. Zhang, D.; Xu, J.; Zhao, Q.; Cheng, T.; Liu, G. A Site-Isolated Organoruthenium-/Organopalladium-Bifunctionalized Periodic Mesoporous Organosilica Catalyzes Cascade Asymmetric Transfer Hydrogenation and Suzuki Cross-Coupling. *ChemCatChem* **2014**, *6*, 2998–3003. [CrossRef]
85. Deng, B.; Xiao, W.; Li, C.; Zhou, F.; Xia, X.; Cheng, T.; Liu, G. Imidazolium-based organoiridium-functionalized periodic mesoporous organosilica boosts enantioselective reduction of α-cyanoacetophenones, α-nitroacetophenones, and β-ketoesters. *J. Catal.* **2014**, *320*, 70–76. [CrossRef]
86. Reid, L.M.; Crudden, C.M. Installing stable molecular chirality within the walls of periodic mesoporous organosilicas via self assembly. *Chem. Mater.* **2016**, *28*, 7605–7612. [CrossRef]
87. Hao, T.T.; Shi, J.Y.; Zhuang, T.Y.; Wang, W.D.; Li, F.C.; Wang, W. Mesostructure-controlled synthesis of chiral norbornane-bridged periodic mesoporous organosilicas. *RSC Adv.* **2012**, *2*, 2010–2014. [CrossRef]

88. Baleizao, C.; Gigante, B.; Das, D.; Alvaro, M.; Garcia, H.; Corma, A. Synthesis and catalytic activity of a chiral periodic mesoporous organosilica (ChiMO). *Chem. Commun.* **2003**, 1860–1861. [CrossRef]
89. Baleizão, C.; Gigante, B.; Das, D.; Álvaro, M.; Garcia, H.; Corma, A. Periodic mesoporous organosilica incorporating a catalytically active vanadyl Schiff base complex in the framework. *J. Catal.* **2004**, *223*, 106–113. [CrossRef]
90. Benitez, M.; Bringmann, G.; Dreyer, M.; Garcia, H.; Ihmels, H.; Waidelich, M.; Wissel, K. Design of a chiral mesoporous silica and its application as a host for stereoselective di-π-methane rearrangements. *J. Org. Chem.* **2005**, *70*, 2315–2321. [CrossRef]
91. Jiang, D.; Yang, Q.; Yang, J.; Zhang, L.; Zhu, G.; Su, W.; Li, C. Mesoporous Ethane−Silicas Functionalized with trans-(1R,2R)-Diaminocyclohexane as Heterogeneous Chiral Catalysts. *Chem. Mater.* **2005**, *17*, 6154–6160. [CrossRef]
92. Jiang, D.; Yang, Q.; Wang, H.; Zhu, G.; Yang, J.; Li, C. Periodic mesoporous organosilicas with trans-(1R,2R)-diaminocyclohexane in the framework: A potential catalytic material for asymmetric reactions. *J. Catal.* **2006**, *239*, 65–73. [CrossRef]
93. Garcia, R.A.; van Grieken, R.; Iglesias, J.; Morales, V.; Gordillo, D. Synthesis of Chiral Periodic Mesoporous Silicas Incorporating Tartrate Derivatives in the Framework and Their Use in Asymmetric Sulfoxidation. *Chem. Mater.* **2008**, *20*, 2964–2971. [CrossRef]
94. Zhang, L.; Liu, J.; Yang, J.; Yang, Q.; Li, C. Tartardiamide-Functionalized Chiral Organosilicas with Highly Ordered Mesoporous Structure. *Chem. Asian J.* **2008**, *3*, 1842–1849. [CrossRef]
95. Wang, P.; Liu, X.; Yang, J.; Yang, Y.; Zhang, L.; Yang, Q.; Li, C. Chirally functionalized mesoporous organosilicas with built-in BINAP ligand for asymmetric catalysis. *J. Mater. Chem.* **2009**, *19*, 8009–8014. [CrossRef]
96. Liu, X.; Wang, P.; Yang, Y.; Wang, P.; Yang, Q. (R)-(+)-Binol-Functionalized Mesoporous Organosilica as a Highly Efficient Pre-Chiral Catalyst for Asymmetric Catalysis. *Chem. Asian J.* **2010**, *5*, 1232–1239. [CrossRef]
97. Polarz, S.; Kuschel, A. Preparation of a periodically ordered mesoporous organosilica material using chiral building blocks. *Adv. Mater.* **2006**, *18*, 1206–1209. [CrossRef]
98. Ide, A.; Voss, R.; Scholz, G.; Ozin, G.A.; Antonietti, M.; Thomas, A. Organosilicas with Chiral Bridges and Self-Generating Mesoporosity. *Chem. Mater.* **2007**, *19*, 2649–2657. [CrossRef]
99. Inagaki, S.; Guan, S.; Yang, Q.; Kapoor, M.P.; Shimada, T. Direct synthesis of porous organosilicas containing chiral organic groups within their framework and a new analytical method for enantiomeric purity of organosilicas. *Chem. Commun.* **2008**, 202–204. [CrossRef]
100. Morell, J.; Chatterjee, S.; Klar, P.J.; Mauder, D.; Shenderovich, I.; Hoffmann, F.; Froba, M. Synthesis and characterization of chiral benzylic ether-bridged periodic mesoporous organosilicas. *Chem. Eur. J.* **2008**, *14*, 5935–5940. [CrossRef]
101. Beretta, M.; Morell, J.; Sozzani, P.; Froeba, M. Towards peptide formation inside the channels of a new divinylaniline-bridged periodic mesoporous organosilica. *Chem. Commun.* **2010**, *46*, 2495–2497. [CrossRef]
102. Zhuang, T.Y.; Shi, J.Y.; Ma, B.C.; Wang, W. Chiral norbornane-bridged periodic mesoporous organosilicas. *J. Mater. Chem.* **2010**, *20*, 6026–6029. [CrossRef]
103. Wang, D.S.; He, J.B.; Rosenzweig, N.; Rosenzweig, Z. Superparamagnetic Fe2O3 Beads-CdSe/ZnS quantum dots core-shell nanocomposite particles for cell separation. *Nano Lett.* **2004**, *4*, 409–413. [CrossRef]
104. Pankhurst, Q.A.; Connolly, J.; Jones, S.K.; Dobson, J. Applications of magnetic nanoparticles in biomedicine. *J. Phys. D Appl. Phys.* **2003**, *36*, R167–R181. [CrossRef]
105. Neuberger, T.; Schoepf, B.; Hofmann, H.; Hofmann, M.; Von Rechenberg, B. Superparamagnetic nanoparticles for biomedical applications: Possibilities and limitations of a new drug delivery system. *J. Magn. Magn. Mater.* **2005**, *293*, 483–496. [CrossRef]
106. Lu, A.-H.; Salabas, E.L.; Schüth, F. Magnetic Nanoparticles: Synthesis, Protection, Functionalization, and Application. *Angew. Chem. Int. Ed.* **2007**, *46*, 1222–1244. [CrossRef] [PubMed]
107. Zhu, Y.; Stubbs, L.P.; Ho, F.; Liu, R.; Ship, C.P.; Maguire, J.A.; Hosmane, N.S. Magnetic Nanocomposites: A New Perspective in Catalysis. *ChemCatChem* **2010**, *2*, 365–374. [CrossRef]
108. Akbarzadeh, A.; Samiei, M.; Davaran, S. Magnetic nanoparticles: Preparation, physical properties, and applications in biomedicine. *Nanoscale Res. Lett.* **2012**, *7*, 1–13. [CrossRef] [PubMed]

109. Zhang, D.; Zhou, C.; Sun, Z.; Wu, L.-Z.; Tung, C.-H.; Zhang, T. Magnetically recyclable nanocatalysts (MRNCs): A versatile integration of high catalytic activity and facile recovery. *Nanoscale* **2012**, *4*, 6244–6255. [CrossRef]
110. Mrowczynski, R.; Nan, A.; Liebscher, J. Magnetic nanoparticle-supported organocatalysts—An efficient way of recycling and reuse. *RSC Adv.* **2014**, *4*, 5927–5952. [CrossRef]
111. Rossi, L.M.; Costa, N.J.S.; Silva, F.P.; Wojcieszak, R. Magnetic nanomaterials in catalysis: Advanced catalysts for magnetic separation and beyond. *Green Chem.* **2014**, *16*, 2906–2933. [CrossRef]
112. Polshettiwar, V.; Luque, R.; Fihri, A.; Zhu, H.; Bouhrara, M.; Basset, J.-M. Magnetically Recoverable Nanocatalysts. *Chem. Rev.* **2011**, *111*, 3036–3075. [CrossRef]
113. Wang, D.; Astruc, D. Fast-Growing Field of Magnetically Recyclable Nanocatalysts. *Chem. Rev.* **2014**, *114*, 6949–6985. [CrossRef] [PubMed]
114. Arakawa, Y.; Chiba, A.; Haraguchi, N.; Itsuno, S. Asymmetric Transfer Hydrogenation of Aromatic Ketones in Water using a Polymer-Supported Chiral Catalyst Containing a Hydrophilic Pendant Group. *Adv. Synth. Catal.* **2008**, *350*, 2295–2304. [CrossRef]
115. Massart, R. Preparation of Aqueous Magnetic Liquids in Alkaline and Acidic Media. *IEEE Trans. Magn.* **1981**, *17*, 1247–1248. [CrossRef]